On the wind-driven circulation in an ocean with bottom topography

By WILLIAM R. HOLLAND, *Scripps Institution of Oceanography, University of California, San Diego*

(Manuscript received January 1, 1967)

ABSTRACT

The influence of bottom topography on the wind-driven ocean circulation is investi gated for a homogeneous, β-plane model with an imposed, steady wind stress curl. The linear model studied by Munk (1950) and the non-linear model studied by Carrier & Robinson (1962) are special cases as is the simple model proposed by Warren (1963) foı the description of Gulf Stream meanders. Although the effects of density stratification are neglected, inertial and frictional effects are included and solutions determined for various kinds of topography.

Simple analytic models are examined and found to be useful in describing limited regions of the ocean basin. In particular the concept of an interior regime, in which non-linear and frictional terms are unimportant, can be extended to the case of variable depth. In regions of strong inertial flow over topography, the simple meander model investigated by Rossby (1940) has some success in predicting the path of the stream. In both models the importance of isopleths of constant F/H, where F is the Coriolis parameter and H is the depth, is demonstrated by showing that there is a strong tendency for streamlines to follow or meander about such curves.

Complete numerical solutions are found for the finite difference vorticity equation by an efficient relaxation scheme developed for this purpose. Results show that the response of the ocean may be strongly controlled by the shape of the ocean bottom and that such gross features of the ocean circulation as Gulf Stream separation, meandering, and variable transport may be related to topograpic effects.

1. Introduction

Within the last few years, a wide variety of investigations has been made concerning the problem of the wind-driven ocean circulation. These have been stimulated by the successes and the inadequacies of models proposed by numerous investigators in the last two decades. In reviewing this work one is struck by the fact that much of the importance of each model lies in the questions it raises regarding its own validity. The frictional theories lead to the result that the neglected non-linear terms are important. A completely inertial theory is found to be untenable when a small amount of lateral friction is put in. The numerical model studied by Bryan does not lead to separation of the boundary current from the coast. These very inadequacies, however, suggest those physical processes which can no longer be ignored and subsequent more realistic oceanic models will have to incorporate them.

Several recent investigations have been made concerning the relative role of inertial and frictional effects. For the case of lateral friction analytic results (Il'in & Kamenkovich, 1963; Moore, 1963) are supported by the numerical investigation of Bryan (1963), showing that at small Reynolds numbers the solution is essentially that of Munk while at large Reynolds numbers steady, Rossby wave type motions become important in the northern half basin. For a model with bottom friction, Veronis (1966) has shown that the frictional solution of Stommel transforms with increasing non-linearity into a solution very much like that of Fofonoff's completely inertial model. We shall be concerned with furthering our understanding of the lateral friction model in the present investigation.

Other recent papers have raised a question that has been much neglected in oceanography: how does the bottom topography affect large scale motions? Greenspan (1963), interested in a criterion for the existence of inertial boundary layers, finds that topography can play an important role, at least in the case of a single homogeneous layer. Warren (1963) finds a definite correlation between the path of the Gulf Stream and bottom topography so that the total circulation pattern may be quite sensitive to the shape of the ocean bottom. Finally, Welander (1959) points out that the density field may not compensate completely and noticeable velocities may occur near the bottom. These results suggest that the assumption of no motion near the bottom of the ocean needs review and that the influence of topography needs to be more fully understood.

The present investigation is an attempt to look more carefully into the inertial-frictional problem and to assess the role played by topography in the large scale, wind-driven ocean circulation. We shall use numerical techniques to find steady solutions to the equation describing the vorticity balance in a homogeneous ocean. The Munk (1950) and Carrier–Robinson (1962) vorticity equations are special cases as is the simple vorticity balance suggested by Warren for the meandering Gulf Stream.

2. The topographic equations

Although the ocean is highly baroclinic, theoretical investigations of the large scale circulation have been concerned for the most part with barotropic or homogeneous models so that a two dimensional problem may be solved. We are forced here to follow suit, realizing fully the inadequacy of such a model in treating realistic oceanic motions. In particular the manner in which the ocean "feels" the bottom is strongly dependent upon the nature of the density field (Holland, 1966) and our knowledge of the situation in the ocean is not adequate at present to realistically take this into account. We proceed then by studying simple model situations which will allow us to isolate some of the physical processes in question so that later they may be incorporated into a more realistic model.

The integrated equations of steady motion, applicable to a homogeneous ocean driven by the wind, have the form

$$uu_x + vu_y - fv = -\frac{1}{\varrho} p_x + A_H \nabla^2 u + \frac{\tau^x}{\varrho h}, \qquad (1)$$

$$uv_x + vv_y + fu = -\frac{1}{\varrho} p_y + A_H \nabla^2 v + \frac{\tau^y}{\varrho h}, \qquad (2)$$

$$(uh)_x + (vh)_y = 0, \qquad (3)$$

where $u(x, y)$ and $v(x, y)$ are the eastward (x) and northward (y) velocity components; $f = f_0 + \beta y$ is the Coriolis parameter for the β-plane; p is the pressure; A_H is the coefficient of horizontal eddy diffusivity, assumed constant; ϱ is the density; h is the depth of the ocean; and τ^x and τ^y are the eastward and northward components of the wind stress. Subscripts denote differentiation. Equations (1) and (2) are the integrated forms of the momentum equations, and (3) is the continuity equation.

The vorticity equation derived from these equations can be put in the form

$$-\psi_y \left(\frac{\zeta + f}{h}\right)_x + \psi_x \left(\frac{\zeta + f}{h}\right)_y = A_H \nabla^2 \zeta + \left(\frac{\tau^y}{h}\right)_x - \left(\frac{\tau^x}{h}\right)_y, \qquad (4)$$

where we have introduced a mass transport stream function, $\psi_x = \varrho vh$ and $\psi_y = -\varrho uh$. The vorticity is given by $\zeta = v_x - u_y = \nabla \cdot (\nabla \psi / \varrho h)$.

We will seek solutions to equation (4) for a variety of topographies and for various degrees of frictional and inertial influence. For convenience we choose the oceanic basin to be square with sides of length L so that $0 \leqslant x \leqslant L$ and $0 \leqslant y \leqslant L$. The wind-stress is assumed to have the simple form used by Stommel (1948), $\bar{\tau} = (-\tau_0 \cos(\pi y/L), 0)$. In order to isolate the important parameters of the problem equation (4) is nondimensionalized by the following scheme:

$$\frac{x}{L}, \frac{y}{L} = X, Y,$$

$$\frac{h}{D} = H,$$

$$\frac{f}{\beta L} = F = F_0 + Y,$$

$$\frac{\beta \psi}{\tau_0 \pi} = \Psi,$$

where D is taken to be the abyssal depth (i.e. the greatest depth in the basin), $\beta = (2\Omega/a)\cos\theta_0$,

$F_0 = (a/L) \tan \theta_0$, Ω = rate of rotation of the earth, a = radius of the earth, and θ_0 is the latitude corresponding to the southern boundary of the basin. For parameters corresponding to the North Atlantic $F_0 = 1.85$. The nondimensional vorticity, Z, is given by

$$Z = \left(\frac{\Psi_X}{H}\right)_X + \left(\frac{\Psi_Y}{H}\right)_Y = \left(\frac{\varrho D\beta L^2}{\tau_0 \pi}\right)\zeta.$$

Equation (4) now takes the form

$$-\Psi_Y\left(\frac{\epsilon Z + F}{H}\right)_X + \Psi_X\left(\frac{\epsilon Z + F}{H}\right)_Y = \delta\nabla^2 Z - \left(\frac{T}{H}\right)_Y, \tag{5}$$

where $\epsilon = \tau_0\pi/\varrho D\beta^2 L^3$, $\delta = A_H/\beta L^3$, and $T = -(\cos \pi Y)/\pi$. This choice of nondimensionalization is convenient in that for the case of constant depth the interior mass transport is of order one, that is $\Psi_x = -\sin \pi Y$. An alternate form of equation (5) is

$$\underset{\mathbf{A}}{\delta H\nabla^2 Z} - \underset{\mathbf{B}}{\epsilon J[\Psi, Z]} - \underset{\mathbf{C}}{\Psi_X} + \underset{\mathbf{D}}{\left(\frac{\epsilon Z + F}{H}\right) J[\Psi, H]} + \underset{\mathbf{E}}{T\frac{H_Y}{H} - T_Y} = 0. \tag{6}$$

We will refer hereafter to term A as the frictional term, term B as the non-linear advective term, term C as the planetary vorticity tendency, term D as the topographic vorticity tendency, and term E as the wind-stress curl. The Jacobian operator $J[F, G]$ means $F_X G_Y - F_Y G_X$.

In order to relate our problem to previous work we note that for Munk's linear problem (H = constant, $\epsilon = 0$) the width of the boundary current is found by assuming a balance between the planetary vorticity term and the frictional term in the boundary layer, that is $\Psi_X \sim \delta \Psi_{XXXX}$. Thus the width of the frictional boundary layer can be defined $W_F = \delta^{\frac{1}{3}}$. To find an inertial boundary width we assume a balance exists between the planetary vorticity tendency and the advection term in the boundary layer, $\epsilon \Psi_{XXY}\Psi_X \sim \Psi_X$. Therefore the width of the inertial boundary layer can be defined $W_I = \epsilon^{\frac{1}{2}}$.

Either pair of parameters, (ϵ, δ) or (W_I, W_F), can be used to define a particular problem. Because of the relevance of the latter to the highly frictional and highly inertial boundary layers we shall choose them. For the complete problem to be studied, however, with topographic, frictional, and inertial effects present the parameters lose their significance as boundary widths, although they still serve as useful numbers in classifying the problem.

3. The Topographic–Sverdrup interior

Sverdrup (1947) derived a relationship which may be applied to the "interior" of the ocean. If the inertial terms and horizontal friction can be neglected in some region of our model ocean and if the depth is constant the vorticity equation (5) takes the simple form

$$\Psi_X = -\sin \pi Y. \tag{7}$$

Hence the north-south mass transport Ψ_X is determined directly from a knowledge of the wind-stress curl. The east-west mass transport $-\Psi_Y$ cannot be determined without further knowledge of the velocity field, since equation (7) gives only the eastward *rate of change* of the east-west mass transport: $-\Psi_{YX} = \pi \cos \pi Y$. Knowing Ψ_Y at some longitude, however, we can integrate this expression along a line of constant latitude to determine the full interior flow field.

Sverdrup's method is equivalent to integrating the first order, partial differential equation (7) along characteristics, in this case lines of constant latitude (F = constant), starting from known values of the function along a curve intersecting the characteristics. For example, the Stommel (1948) interior flow in a square basin can be calculated, assuming the simple relationship (7) to hold right up to the eastern boundary. We find by integration

$$\Psi(X,Y) = (1-X)\sin \pi Y, \tag{8}$$

where the integration constant has been determined by specifying Ψ on the eastern boundary, $\Psi(1, Y) = O$. This interior solution cannot satisfy the western boundary condition, $\Psi(O, Y) = 0$, and a western boundary layer in which frictional or non-linear terms become important is needed to complete the solution.

The foregoing development is a review of the nature of the Sverdrup balance and of its incorporation into the wind-driven theories. Now let us examine the effect of variable depth on the Sverdrup balance in a homogeneous, single layer ocean, that is, let us look at a *Topographic–Sverdrup Interior*. The vorticity equation has the form

$$-\Psi_Y\left(\frac{F}{H}\right)_X + \Psi_X\left(\frac{F}{H}\right)_Y = \left(\frac{\cos \pi Y}{\pi H}\right)_Y. \quad (9)$$

The north-south mass transport is no longer specified by the wind-stress curl, but this first order, partial differential equation can still be solved by integrating ordinary differential equations along characteristics. Thus if the curve $X(S), Y(S)$, determined from the simultaneous differential equations

$$\frac{dX}{dS} = -\left(\frac{F}{H}\right)_Y, \quad \frac{dY}{dS} = \left(\frac{F}{H}\right)_X, \quad (10)$$

can be found, Ψ can be determined along the characteristic by integrating

$$\frac{d\Psi}{dS} = -\left[\frac{\cos \pi Y(S)}{\pi H(X(S),\, Y(S))}\right]_Y. \quad (11)$$

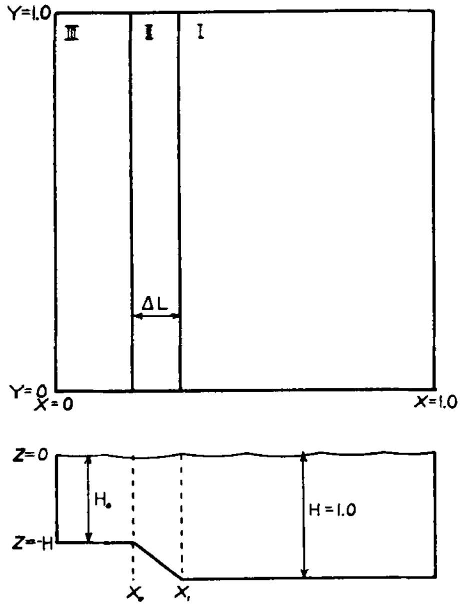

Fig. 1. The topographic model for which Topographic–Sverdrup interior solutions are calculated.

It is clear from equation (10) that the characteristics are lines of constant F/H. In fact, if the wind-stress term is unimportant, the flow itself would be along these lines. A column of fluid moving northward would have to enter deeper water while one moving southward would have to enter shallower water. We shall find ample evidence for behavior of this sort in our model and shall be interested in the deviation from it with increasing non-linearity.

For complex topography the above integrations are most easily accomplished by a graphical method. Assuming as before a square basin, $0 \leqslant X \leqslant 1$, $0 \leqslant Y \leqslant 1$, whose boundary forms the streamline $\Psi = 0$, we begin at a position on the eastern boundary (ignoring the possibility of frictional and inertial boundary layers there). The procedure then is to choose a suitably small ΔS (small with respect to the scale of variation in F/H) and calculate the stream function at a series of positions (X, Y) along the characteristic using equations (10) and (11).

The solution in those regions of the basin not entered by characteristics from the eastern boundary must be calculated by following characteristics beginning on the north or south boundary. Note that the entire procedure gives "correct" values of the stream function only as long as the characteristic does not pass through a region in which fricton or inertial terms are important. In fact we are using our knowledge that the western boundary region is the site for large frictional and inertial effects to choose the eastern boundary as the starting point for our calculations. We shall see that this leads to good results for the interior solution of the Munk model, with due respect for the minor frictional eastern boundary current in Munk's solution. In the topographic model the test is to compare the "interior" solutions with full solutions determined numerically.

In order to illustrate the above procedure and to test to what extent a solution is governed by a Topographic–Sverdrup balance, let us look at the following example. The topography consists of three regions (Fig. 1), an eastern region of constant depth $H = 1.0$, a slope region in which the depth varies linearly according to $H = \gamma(X - X_1) + 1$, and a western boundary shelf of constant depth H_0. The gradient in the region of topographic variation is given by $\gamma = (1 - H_0)/\Delta L$ where $\Delta L = X_1 - X_0$.

The solutions in the three regions are now easily found by the above procedure. In fact because of the simplicity of our example, the equations may be integrated exactly and analy-

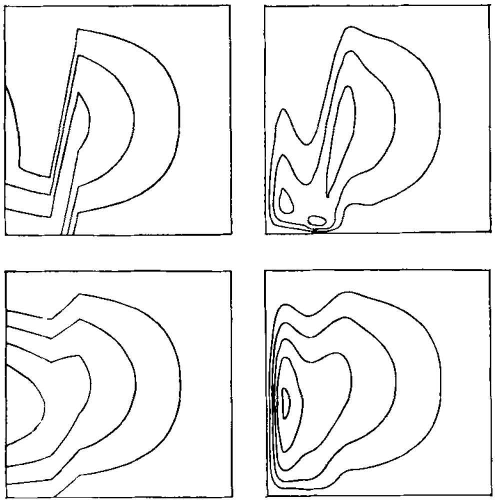

Fig. 2. Mass transport streamlines of the Topographic–Sverdrup interior solution for two cases (*upper left* and *lower left*) with differing topography. The slope region II of Figure 1 is five times as steep for the upper solution as for the lower one. Also shown, on the right, are complete numerical solutions ($W_I = 0.005$, $W_F = 0.025$) for the same topographies.

tic solutions obtained. In particular the solutions in the eastern and western regions of constant depth are just those of Sverdrup and the characteristics are the straight lines $Y =$ constant.

In the region of variable depth it is easily shown that $F/H =$ constant leads to $(X - X_e) = (Y - Y_e)/\gamma F_e$, the subscript e identifying a given characteristic in terms of values at the eastern edge of the region. The characteristic here is also a straight line the slope of which is given by γFe, proportional to the topographic slope and the value of the Coriolis parameter at the eastern edge of the region (where the characteristic first turns southward). The larger the topographic slope, the greater is the southward penetration of the characteristic per unit decrease in X.

Let us now compare the Topographic–Sverdrup solution for the above example with the full numerical solution in which frictional and inertial effects close the flow. Figure 2 shows the Topographic–Sverdrup interior solution and the full numerical solution ($W_F = 0.025$, $W_I = 0.005$) for two cases with differing topography. The lower solutions are those with topography for which $\gamma = 0.05/\Delta L$ while for the upper solutions $\gamma = 0.25/\Delta L$. Thus the variable topography is five times as steep for the upper figures as for the lower ones. Note that the Topographic–Sverdrup solution gives a quite good representation of the flow field except in the vicinity of sharp changes in topography and of course in the vicinity of boundaries where the solution does not satisfy the boundary conditions.

In general, then, we find that the Sverdrup method may be extended to include topographic effects, and the "interior" solution so calculated deviates only in minor details from the full solution, at least for these values of the parameters W_I and W_F. For larger values of W_I or W_F we expect the interior region to become less extensive, the inertial and frictional effects not being confined to such a small boundary region.

4. The frictional–inertial boundary layer

Some insight into the nature of the frictional–inertial boundary layer may be obtained by extending an investigation by Moore (1963). For simplicity the depth is assumed constant so that equation (6) has the form

$$W_I^2(-\Psi_Y Z_X + \Psi_X Z_Y) + \Psi_X = W_F^3 H \nabla^4 \Psi - \sin \pi Y. \qquad (12)$$

Following Moore we assume that the stream function has a boundary layer character near the western wall $X = 0$ so that $\delta/\delta X >> \delta/\delta Y$, and furthermore we linearize the equation by replacing $-\Psi_Y Z_X + \Psi_X Z_Y$ by $M(Y) Z_X$, where M is the east–west component of the *interior* mass transport near the western wall. Then writing $\Psi = \Psi^* \sin \pi Y$, the model equation becomes

$$W_F^3 \Psi^*_{XXXX} - W_I^2 M(Y) \Psi^*_{XXX} - \Psi^*_X - 1 = 0. \qquad (13)$$

with boundary conditions $\Psi^* = \Psi^*_X = 0$ on $X = 0$ and $X = 1$.

Thus the non-linear, partial differential equation (12) has been replaced by a linear, ordinary differential equation with a parametric Y dependence. The second term in (13) contains the only remaining non-linear effect, the east–west transport of relative vorticity by the interior flow. The north–south transport of vorticity is neglected. We justify this procedure by pointing out that our aim is to begin to understand the interaction of inertial and frictional effects in the boundary layer in a very simple context. Whether such results have application to the complete model remains to be seen. A comparison of those features of the boundary layer predicted by this simple model with the complete numerical solutions will be useful in this regard.

The main point of our study of equation (13) will be to understand the differences in the nature of the boundary layer in the northern and southern half basins as a result of the change in sign of $M(Y)$. In the northern half of the basin the mass transport is away from the western boundary so that $M(Y) > 0$, while in the southern half the mass transport is toward the western boundary, $M(Y) < 0$. This difference has an important influence on the nature of the flow for sufficiently large inertial effects, i.e. for W_I sufficiently large. For W_I very small, we shall find that the solution reduces to Munk's results.

Equation (13) has the general solution

$$\Psi^* = -X + \sum_{i=1}^{3} A_i e^{-\lambda_i X} + A_0, \tag{14}$$

where the A_i are constants to be determined from the boundary conditions, and the λ_i are roots of the cubic equation

$$W_F^3 \lambda^3 + W_I^2 M(Y) \lambda^2 + 1 = 0. \tag{15}$$

There are two limits of this equation which are relevant to previous wind-driven circulation models. If we assume $W_I = 0$ we have $\lambda^3 = -W_F^{-3}$ that is $\lambda_1 = -1/W_F$, $\lambda_{2,3} = \frac{1}{2}(1 \pm \sqrt{3}i)/W_F$. The results are equivalent to Munk's (1950). In particular the western boundary solution has a decay rate $d_r = 1/(2W_F)$ and an oscillation wave number $k = \sqrt{3}/(2W_F)$. The western boundary solution has the form $e^{-d_r X} \cos(kX + \theta_0)$. Note that there is symmetry about $Y = 0.5$, that d_r and k are independent of Y.

If in (15) $W_F = 0$ we have $\lambda^2 = -[W_I^2 M]^{-1}$. For $M(Y) > 0$ (northern half basin) $\lambda = \pm i/(W_I \sqrt{M})$. The solution is entirely oscillatory. Rossby waves, able only to travel towards the west, may stand still on an eastward flowing current. For $M(Y) < 0$ (southern half basin) $\lambda = \pm 1/(W_I \sqrt{|M|})$. The solution is entirely exponential in character. The latter solution was used by Fofonoff (1954) to construct free inertial solutions to the frictionless equations of motion.

Let us now examine the complete cubic, equation (15). It can be shown (Conkwright, p. 74) that this equation has one negative real root and two complex conjugate roots with a positive real part when $M(Y) > -(27/4)^{\frac{1}{3}} (W_F/W_I)^2$. When $M - (27/4)^{\frac{1}{3}} (W_F/W_I)^2$ the roots are all real, one being negative and two positive. The complex conjugate roots in the first case and the two positive roots in the second are the parameters relevant to the behavior of the western boundary layer and will be examined closely.

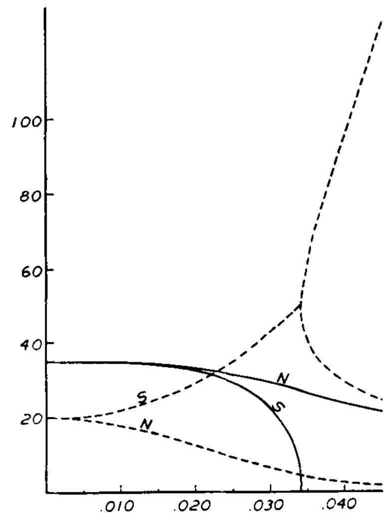

Fig. 3. The decay rates, d_r (dashed curves), and wave numbers, k (solid curves) of the spatial oscillation for the northern (N) and southern (S) half basins as a function of the inertial parameter W_I. W_F is fixed at 0.025.

The interior east–west mass transport at the western boundary is, according to equation (8), $M(Y) = -\pi \cos \pi Y$. For convenience in calculation the pair of Y-values (equal distance from the midlatitude, $Y = 0.5$) at which $M = \pm 2$ is chosen. The plus sign goes with the northern half basin, and the minus sign with the southern half basin. Equation (15) can now be solved for a series of W_I values (W_F fixed at 0.025) in order to examine how the decay constant and oscillation wave number for the western boundary layer vary with increasing non-linearity.

Figure 3 summarizes the results. The decay rates d_r (dashed curves) and the oscillation wave numbers k (solid lines) for the northern (N) and southern (S) half basins are plotted. For $W_I = 0$ we find the Munk decay rate and wave number applicable to our choice of the parameter W_F. There is complete symmetry about $Y = 0.5$. As W_I increases the southern decay rate increases, that is, the boundary layer becomes narrower. In the northern half basin the contrary is true; the boundary layer width becomes larger. Thus when W_I is equal to W_F, the northern boundary width is more than twice the purely frictional width while the sinusoidal dependence has changed only slightly. The result is that although the oscillation shows up only slightly in the Munk solution, the oscillation in the inertio-frictional northern half basin is damped more slowly, and stationary planetary waves manifest themselves. In the southern basin the oscillation is damped much more rapidly than in the frictional problem, and in fact for W_I greater than a critical value there is no oscillation at all. Instead there are two relevant decay rates. We shall return to this point shortly.

It is worth noting that the oscillatory behavior in the northern half of the basin, while more pronounced in the inertio-frictional case, is inherent even in the purely frictional model of Munk. Thus these wave-like motions are *not* Rossby waves in the normal sense, but really stationary inertio-frictional waves. A close look at solutions of the form (14) shows that for moderate values of W_I both friction and nonlinearity are important in a large part of the northern half basin.

South of the maximum of the wind-stress curl we find that for increasing W_I the spatial oscillation becomes less and less important. The western boundary solution decays so rapidly that the spatial oscillation does not have room to manifest itself. Above a critical value of W_I no oscillation exists; instead there are two decay rates. For large W_I it can be shown that one decay rate defines an inertio-frictional subboundary layer in which $d_r \sim W_I^2/W_F^3$, while the other decay rate has the character $d_r \sim 1/W_I$, i.e. it is an inertial boundary current. In the former frictional dissipation of vorticity balances its advection while in the latter the advection of vorticity is balanced by the planetary vorticity tendency. Note that the critical W_I value is given by $W_I^C = (-27/4M^3)^{\frac{1}{4}} W_F$, or for $M(Y) = -2$, $W_I^C \doteq W_F$. Hence two decay rates exist in the south (south of the latitude at which $M(Y) = -2$) when $W_I > W_I^C$ and the inertial boundary layer is wider than the inertio-frictional sublayer by a factor $(W_I/W_F)^3$. For W_I somewhat greater than W_F then, the southern boundary layer has primarily an inertial character and friction is of importance only in a rather narrow region adjacent to the boundary.

Although the model is a very simple one, several surprising and interesting results have come out of it. It is in some sense an extension of Munk's model, but it leads to the conclusion that the inertial theories of Charney and Morgan should give good results in the southern region, except in a narrow region very close to the boundary, when W_I is greater than W_F. It also lends weight to Morgan's suggestion that dissipative effects may be left to the northern region without serious consequence. Finally we see that the wave-like meanders in the northern half basin are rather complex inertio-frictional waves which are present even when the nonlinear terms are ignored completely.

5. The meander mechanism

A simplified form of the vorticity equation (5) was applied by Rossby (1940) to atmospheric models and used by Warren (1963) to provide an explanation for the steady meander patterns of the Gulf Stream northeast of Cape Hatteras. If frictional and driving forces are assumed to be negligible in some limited region of the model ocean, equation (5) has the form

$$-\Psi_Y \left(\frac{\epsilon Z + F}{H}\right)_X + \Psi_X \left(\frac{\epsilon Z + F}{H}\right)_Y = 0. \quad (16)$$

This equation is the mathematical statement that potential vorticity is conserved following mass transport streamlines.

In the 1940's Rossby's results were used in meteorology to compute the trajectories of air parcels, given their initial speed, direction, latitude and path curvature (Fultz, 1945). For constant depth (no convergence or divergence) such trajectories were called *constant absolute vorticity trajectories*. These methods may be extended to include variable depth and so compute what can be called *constant potential vorticity trajectories*. This is essentially what Warren has done in his study of Gulf Stream meanders.

We will not review these results here but will examine the numerical solutions described in the next section to ascertain whether the vorticity balance of equation (16) is the primary one for certain limited regions of the basin. In particular the meandering of the model Gulf Stream after it leaves the coast will be examined to determine to what extent potential vorticity is conserved.

6. Numerical solutions

In previous sections we have developed the full equations and examined simple vorticity balances which may be applicable to restricted portions of the model basin. Now we turn our attention to solving the complete non-linear problem posed by equation (5) together with appropriate boundary conditions. First the numerical technique developed for this purpose is described and some questions concerning convergence and accuracy of the finite difference solution discussed. Then the numerical solutions are discussed for various topographic situations and varying degrees of frictional and inertial influence. Finally some questions regarding the wind-stress distribution and boundary conditions are examined with the intention of beginning to understand the behavior of more complicated systems.

There are many possible numerical schemes for solving equations like (5), but few have been thoroughly explored. One method, however, has been studied extensively by the meteorologist, that of integrating the time dependent equivalent of equation (5) from a state of rest. This method was used to attack the wind-driven circulation problem in a constant depth ocean by Bryan (1963) and by Veronis (1966). While this method gives additional information about the time dependent behavior of the physical system it is not necessarily the most efficient way to obtain *steady* solutions of the problem. Since the topographic problem has an added degree of complexity and full understanding of it requires many solutions with differing topography it was necessary that a more rapid numerical procedure be found.

The method developed for this purpose is a relaxation procedure closely related to the successive overrelaxation procedure (Forsythe & Wasow). We apply this technique to the finite difference equation derived from the differential equation (5). The continuous fields of vorticity, depth, and mass transport stream-function are represented by their values at a finite number of discrete points spaced closely together, while the derivatives of a variable are calculated from the values of the variable at discrete points in the vicinity of the point in question.

For our investigation we select a 41×41 grid so that the spacing between points, Δ, in our unit square basin is 1/40 (Figure 4*a*). Then, the eastward and northward coordinates are written $X = (i-1)\Delta$, $Y = (j-1)\Delta$, i and j taking on values from 1 to 41. The finite difference representation of the vorticity equation (6) is found to be

$$W_F^3 \mathrm{H}_{ij} \mathrm{L}Z + W_I^2 \hat{J}[\Psi, Z] - \delta^X \Psi + (W_I^2 Z_{ij} + F_j)\hat{J}[\Psi, \mathrm{H}]/H_{ij} + T_j \delta^Y H / H_{ij} - \delta^Y T = 0, \tag{17}$$

where

$$\mathrm{L}Z = (Z_{i+1,j} + Z_{i-1,j} + Z_{i,j+1} + Z_{i,j-1} - 4Z_{ij})/\Delta^2,$$

$$\hat{J}[F, G] = [(F_{i+1,j} - F_{i-1,j})(G_{i,j+1} - G_{i,j-1}) - (F_{i,j+1} - F_{i,j-1})(G_{i+1,j} - G_{i-1,j})]/4\Delta^2,$$

$$\delta^X F = (F_{i+1,j} - F_{i-1,j})/2\Delta,$$

$$\delta^Y \mathrm{G} = (G_{i,j+1} - G_{i,j-1})/2\Delta.$$

Equation (17) is an accurate representation of equation (6) to order Δ^2. The vorticity Z_{ij} is given in terms of the Ψ field by

$$Z_{ij} = \frac{\mathrm{L}\Psi}{H_{ij}} - \frac{\delta^X\Psi\delta^X H}{H_{ij}^2} - \frac{\delta^Y\Psi\delta^Y H}{H_{ij}^2}. \tag{18}$$

The boundary conditions used in this investigation are those of Munk, i.e. on $X = 0,1$, $\Psi = \Psi_X = 0$ (noslip condition) and on $Y = 0,1$, $\Psi = \Psi_{YY} = 0$ (slip condition). In terms of the finite difference representation these lead to expressions for Ψ on the boundary and for Z on the boundary in terms of Ψ at interior points.

Let us now outline a recipe describing the iterative relaxation scheme used to solve equation (17).

Step 1: Make an initial guess at the values of Ψ_{ij} and compute initial values of Z_{ij} from equation (18) and the boundary conditions.

Step 2: Sweep through all of the interior points, one by one, accomplishing the following substeps at each:

A point (i, j)

(*a*) Compute a correction to Ψ_{ij} such that equation (17) is approximately satisfied at that point. Over and under-relaxation proves useful in various circumstances.

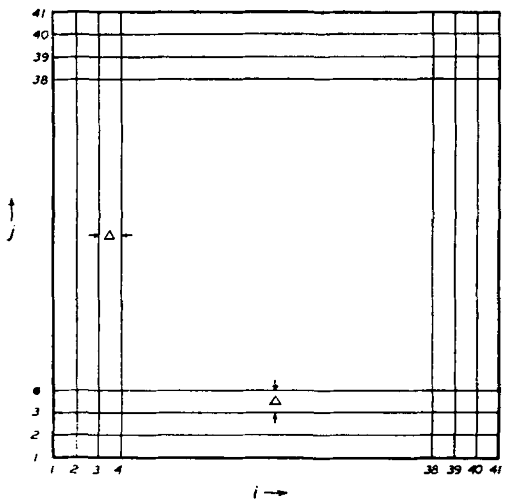

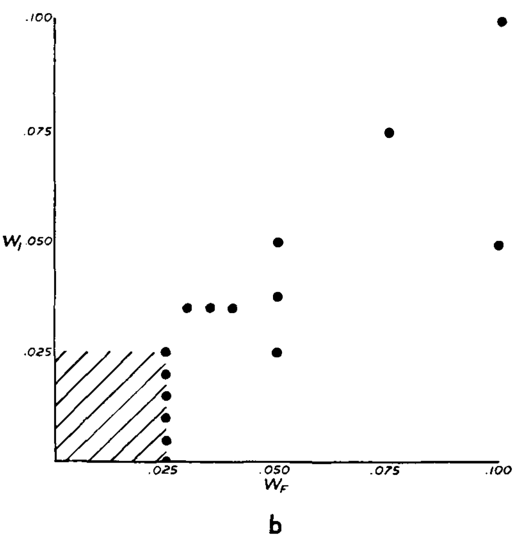

Fig. 4. (*a*) The finite difference grid for our model ocean. (*b*) The variety of solutions found for an ocean of constant depth. Each point in the W_I–W_F plane represents a solution obtained by our relaxation method for the 41×41 grid.

(*b*) Having corrected Ψ_{ij}, make a correction to the Z field at points (i, j), $(i+1,j)$, $(i-1,j)$, $(i,j+1)$ and $(i,j-1)$ so that equation (18), applied at these points, remains satisfied.

Step 3: Determine new boundary values of Z.

Step 4: Test for convergence. Either return to step 2 or go to step 5.

Step 5: End of iterative procedure.

Several schemes other than a direct relaxation of the biharmonic operator have been examined but have not yielded significant improvement. One advantage of the above scheme is that the vorticity field as well as the streamfunction field is corrected at each point successively and that previous corrections are taken into account immediately. The most important advantage, however, is that the boundary layer nature of this problem makes available a good initial guess: the Topographic-Sverdrup interior solution. Only the small scale errors need to be relaxed away.

In any case, the above method gives quite rapid convergence for moderate degrees of nonlinearity, and steady solutions to a wide variety of cases have been obtained. For sufficiently large values of the inertial parameter, however, the method fails to converge; the solution "blows up" at an early stage of the iterative procedure. It has been found experimentally that the critical values of W_I are somewhat greater than the W_F of the problem, although particular topographic regimes seem to stabilize the calculation somewhat. Results found by Bryan suggest that this behavior is associated with a physical instability of the flow and not with the numerical method.

There is a practical limit to the narrowness of the boundary current which can be represented accurately by finite difference methods. It was found for the linear problem that when $W_F \geqslant \Delta$ the streamfunction and vorticity values were accurate to about two per cent. As W_F decreased from Δ however, the accuracy decreased rapidly until, at $W_F = \Delta/2$, errors of 20% or greater were in evidence. It was decided therefore to limit the calculations to cases in which $W_F \geqslant \Delta$. The size of Δ is restricted because the computer time required for convergence increases rapidly with the number of interior points. These considerations led to the selection of the 41×41 grid for which $\Delta = 0.025$. The shaded region of Figure 4*b* indicates therefore the region of the W_I, W_F-plane which is not accessible to us.

Let us now look at the numerical solutions, beginning with constant depth cases which complement those of Bryan. Figure 5 shows a series of solutions for increasing size of the inertial parameter, W_I. The plots show the mass transport streamlines with a constant transport interval. The first solution ($W_I = 0.010$, $W_F = 0.025$) is close to the frictional solution found by Munk. The interio-frictional oscillation, strongly

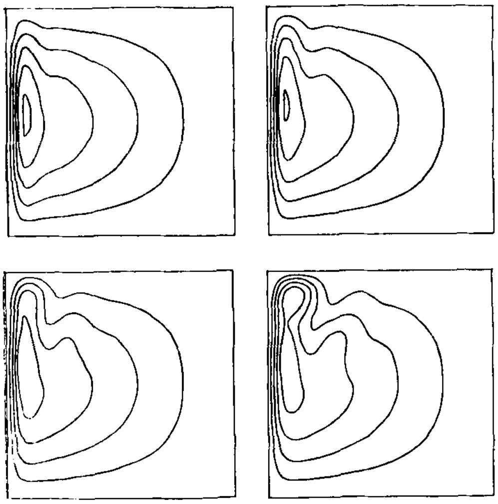

Fig. 5. Mass transport streamlines in an ocean of constant depth for four solutions with increasing values of the inertial parameter (with constant $W_F = 0.025$). *Upper left*: $W_I = 0.010$. *Upper right*: $W_I = 0.015$. *Lower left*: $W_I = 0.020$. *Lower right*: $W_I = 0.025$.

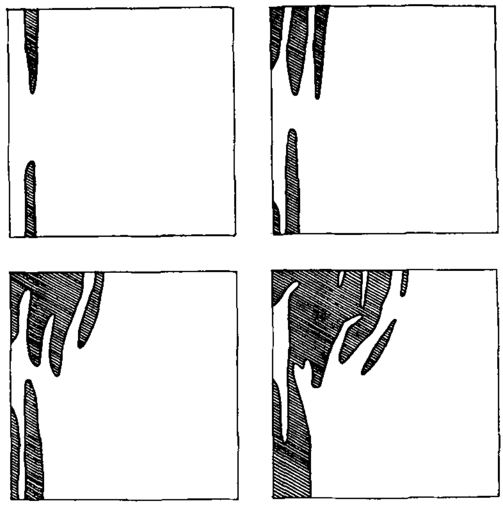

Fig. 7. Regions of significant contribution by the non-linear inertial terms to the vorticity balance (shaded areas) for the sequence of solutions shown in Fig. 5.

frictional in character for this case, shows up quite well in both northern and southern halves of the basin and is nearly symmetrical about the midlatitude. The next case ($W_I = 0.015$, $W_F = 0.025$) begins to show the effect studied analytically in section 4, that is, the spatial oscillation in the northern half basin is becoming more pronounced and that in the southern half basin less

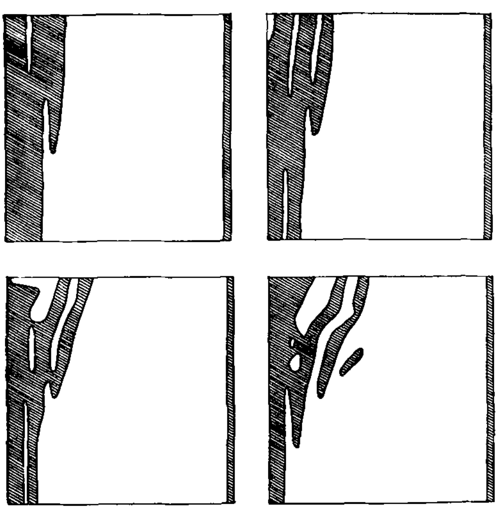

Fig. 6. Regions of important frictional contribution to the vorticity balance (shaded areas) for the series of solutions shown in Fig. 5.

pronounced. In the final pair of solutions, ($W_I = 0.020$, $W_F = 0.025$ and $W_I = 0.025$, $W_F = 0.025$ respectively), the effect becomes more and more extreme, inertio-frictional waves dominating the northern half basin while all indications of oscillatory behavior have disappeared in the south.

These results are graphically illustrated in Figures 6, 7, and 8. Figures 6 and 7 show regions of significant frictional and inertial influence respectively for the set of solutions shown in Figure 5. To determine significance we have established the following quite arbitrary criterion. The terms A, B, C, D and E of equation (6) are ordered in absolute magnitude. For a given term to be significant it must be either first or second largest in magnitude (the primary balance) or, if it is third largest, it must be larger in magnitude than one half of the second largest term.

The shaded regions of Figure 6 are the regions of important frictional contribution to the vorticity balance. The first case is that closest to the linear solution of Munk, but already the effect of the non-linear terms can be seen. The width of the frictional region in the northern half of the basin has become larger than that in the south and, as W_I is increased, this asymmetry is accentuated. Regions (unshaded) near the western boundary appear in which the non-linear advective terms have replaced the frictional term in balancing the planetary vorticity tendency. The oscillatory nature of the solution becomes readily apparent in the northern half of the basin while, in the south, the frictional region becomes narrower. Thus these important features, predicted by Moore's simple analytic model (section 4), are confirmed by the complete numerical solutions.

The role played by the inertial terms for the same sequence of solutions is illustrated in Figure 7. Note that in the north the solution is such that advection and friction alternate in importance in bands oriented in the north–south direction. As W_I increases, the frictional bands become narrower while the inertial ones become wider. In the south the advective terms replace the frictional term in the outer part of the boundary layer, that is, the boundary current becomes primarily an inertial one for large W_I except very near to the boundary where friction and advection are both large. Again the simple model examined earlier is found to give remarkably good results, at least for this range of W_I values.

The Sverdrup interiors which result when the effects of frictional and inertial terms are combined are shown in Figure 8. The unshaded regions are those in which the essential vorticity balance is between the wind-stress curl and the planetary vorticity tendency. As W_I is increased, the width of the non-Sverdrup region increases in the northern part of the basin until a very large part of that half basin is of complex nature. In the south the width of the non-Sverdrup region does not change much although, as we have seen, its nature changes quite markedly.

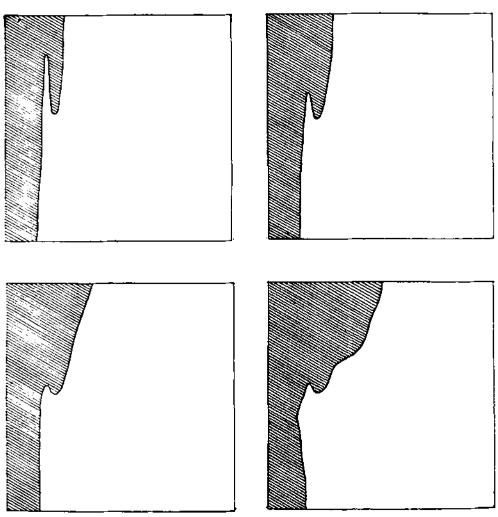

Fig. 8. The Sverdrup interiors (unshaded regions) for the sequence of solutions shown in Fig. 5.

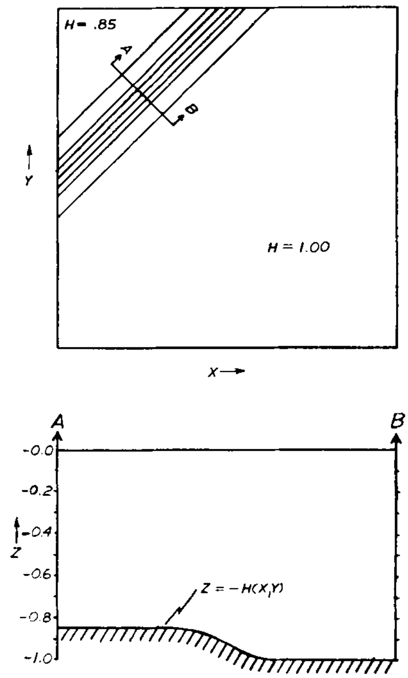

Fig. 9. A topographic regime for which solutions are determined. The depth of the basin is given by $H = 0.925 + 0.075 \tanh (10.0(X-Y-0.5))$. The upper figure shows the model basin with several representative contours drawn. The lower figure shows a cross-section of the region of rapid topographic change.

We begin our examination of the topographic cases by following the procedure used for the constant depth cases, that is, we examine a series of solutions with increasing inertial parameter. The topographic regime is a simple one with a shallow region of constant depth in the northwest corner of the basin connected to the deep ocean by a smooth varying by slope region (Figure 9). Figure 10 shows the mass transport streamlines for steady solutions in which W_I takes on values 0.005, 0.015, 0.020, 0.025 consecutively. W_F is fixed at 0.025.

Note that in all cases the boundary current leaves the coast for this topographic regime. We shall examine more closely the vorticity balance

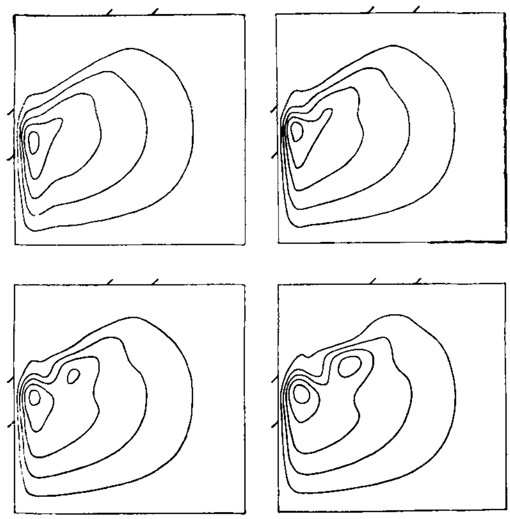

Fig. 10. Mass transport streamlines for steady solutions in the basin with bottom topography shown in Fig. 9. The marks on the boundaries indicate the location of rapid change in depth. The frictional parameter W_F is equal to 0.025. *Upper left*: $W_I = 0.005$. *Upper right*: $W_I = 0.015$. *Lower right*: $W_I = 0.025$. *Lower left*: $W_I = 0.020$.

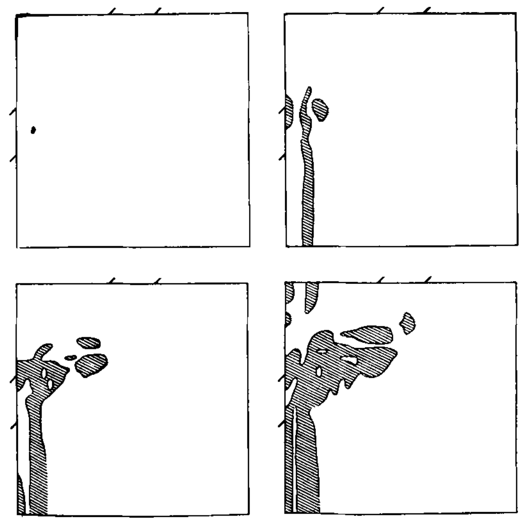

Fig. 12. Regions of significant contribution (shaded areas) by the non-linear advective terms to the vorticity balance for the sequence of solutions shown in Fig. 10. The marks on the boundaries indicate the location of rapid change in depth (see Fig. 9).

in the separation region for the frictional and inertial extremes. A second interesting feature of these solutions is that the narrow current down-stream from separation exhibits meandering that becomes more pronounced as W_I is increased. In the highly frictional case, the stream turns seaward and follows lines of constant F/H, entering deeper water as it moves northward. For the highly inertial regime, the streamline pattern is more complex as meanders and multiple centers of high pressure have become important. We shall examine the rather complicated structure of the solution in this region.

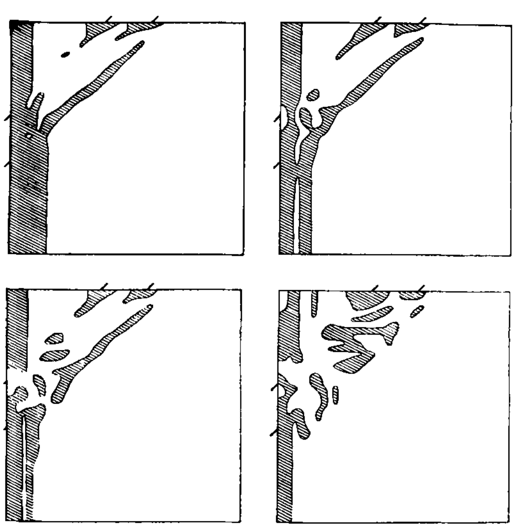

Fig. 11. Regions of important frictional contribution (shaded areas) to the vorticity balance for the series of solutions shown in Fig. 10. The marks on the boundaries indicate the location of rapid change in depth (see Fig. 9).

The information present in this sequence of solutions is displayed in various ways by Figures 11 through 18. The first two of these show regions of important frictional and inertial contribution, respectively, to the vorticity balance. The criterion for determining whether a term is of importance is that it must be one of the two terms making up the primary balance in equation (6), that is, it must be one of the two largest terms in absolute magnitude. In the formation region of the western boundary current the behavior is similar to the flat bottom cases, that is, as W_I is increased the frictional boundary region becomes narrower, the outer region becoming primarily inertial in character. Very close to the boundary, advective terms are balanced by frictional dissipation.

As the boundary current impinges upon the topographic slope region, horizontal divergence occurs, and the topographic terms in the vorticity equation become large. For the highly frictional problem (W_I small) the frictional term becomes large in this region to balance the topographic term while, for W_I large, the inertial terms play this role. In all cases the stream turns seaward to follow the topographic contours.

Following separation the stream enters a region of strong topographic control. For small W_I the frictional and inertial terms both play a minor role, the vorticity balance being primarily between the topographically induced convergence effect and the planetary vorticity tendency. There is a frictional transition region as the streamlines leave the steep topographic region to join up with the Sverdrup regime where the wind-induced vorticity contribution again becomes important. As W_I is increased the behavior in the slope region becomes more and more complex. The streamlines tend to overshoot their equilibrium F/H line and meander about it. Over large parts of the slope region the vorticity balance is that discussed by Warren although, for the range of parameters studied, friction is still of some importance downstream from separation.

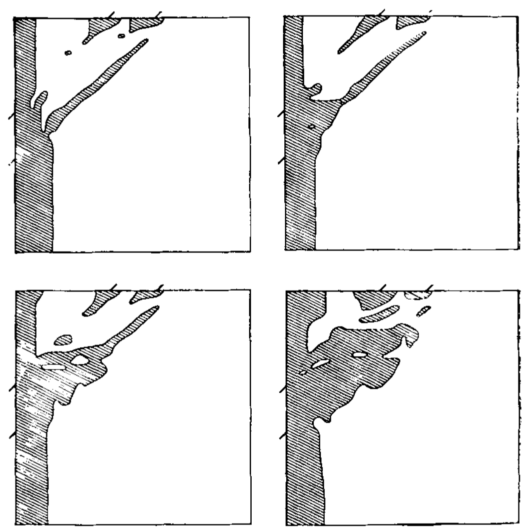

Fig. 14. The Topographic-Sverdrup interior region (unshaded). The vorticity balance is between the wind-stress curl, the planetary vorticity tendency, and the topographic vorticity tendency. The marks on the boundaries indicate the location of rapid change in depth (see Fig. 9).

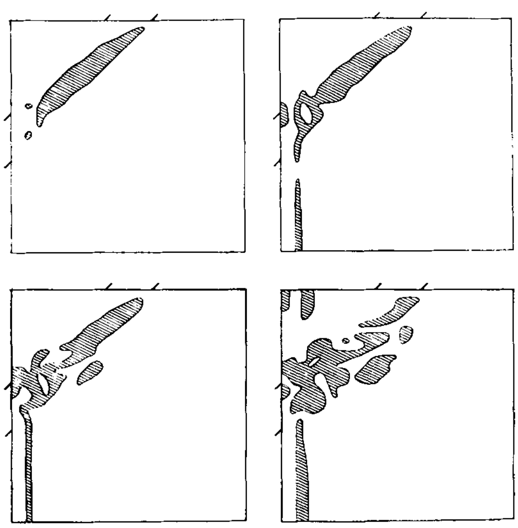

Fig. 13. Regions (shaded) in which the balance of terms is primarily that studied by Warren for Gulf Stream meanders. The potential vorticity following a streamline is nearly constant in this region. Frictional and wind stress-induced vorticity are unimportant. The marks on the boundaries indicate the location of rapid change in depth (see Fig. 9).

Figure 13 shows those regions (shaded) in which the vorticity balance is primarily that studied by Warren. As long as a streamline remains in this region, its potential vorticity is nearly conserved. We find a tendency for this region to increase in extent as W_I is increased, although as meandering becomes extreme the region tends to be interrupted by frictional regions. In any case an extensive part of the solution is governed by conservation of potential vorticity, and we find meanders to be naturally occuring phenomena in a wind-driven model ocean with bottom topography.

The Topographic–Sverdrup interior region is shown in Figure 14. The unshaded portions of the basin are those in which the vorticity balance is between the windstress curl, the planetary vorticity tendency, and the topographic vorticity tendency. For W_I small the departure from the Topographic–Sverdrup balance, mainly frictional, occurs near the western boundary and along the edge of the topographic region. For large W_I both frictional and inertial effects become important in the formation region and in the meander region northeast of the separation point.

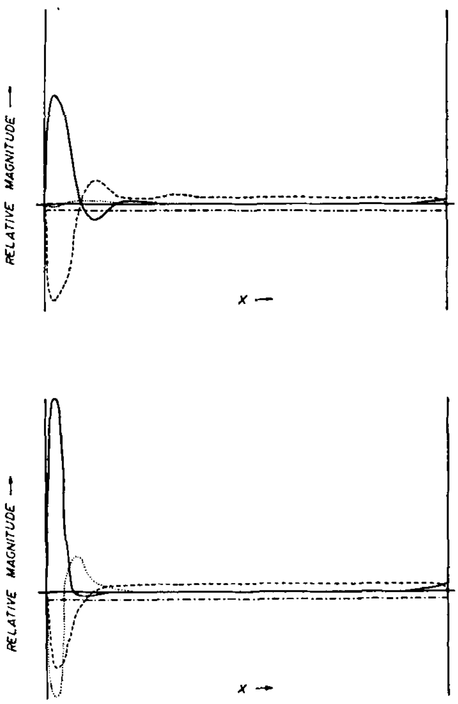

Fig. 15. An east–west cross-section showing the balance of terms in the vorticity equation (6) at a latitude corresponding to the formation region of the western boundary current, $Y = 0.25$. W_F equals 0.025. The topographic term D of equation (6) is identically zero along this cross-section. *Upper*: $W_I = 0.005$. *Lower*: $W_I = 0.025$. ——, frictional term; – – – –, planetary vorticity tendency; . . . ., advective terms; –.–.–.–, wind stress curl.

The differences between the two extreme cases ($W_I = 0.005$ and $W_I = 0.025$) are further illustrated in Figures 15 and 16. Figure 15 shows the balance of terms in the vorticity equation (6) as a function of the eastward coordinate for a value of Y equal to 0.25, that is, for a latitude intersecting the formation region of the western boundary current. For $W_I = 0.005$ we find the situation explored by Munk, a narrow northward flowing current near the boundary and a southward flowing counter current to the east. Frictional diffusion of vorticity balances the planetary vorticity tendency in these regions. Further eastward the planetary vorticity tendency is balanced by the vorticity input by the wind. For $W_I = 0.025$ the situation is somewhat different. The inertial term has become large, reinforcing the planetary vorticity tendency very near the boundary. The resulting frictional dissipation is nearly twice as large there as in the previous case, although the width of the region of important frictional effect has decreased markedly. In the outer part of the boundary region we find a balance between the advection of relative vorticity and the planetary vorticity tendency, the situation studied by Charney (1955) and by Morgan (1956). There is no counter current as in the frictional case; all transport is northward until the Sverdrup regime is met.

Figure 16 shows the balance of terms for a value of Y equal to 0.625, that is, for a latitude slightly northward of the separation region. Here the topographic term plays an important role in the region of the rapidly sloping bottom, contributing in a negative sense when the stream enters shallow water (see equation 6). In the highly frictional case ($W_I = 0.005$) we find the transport to be northward between the bound-

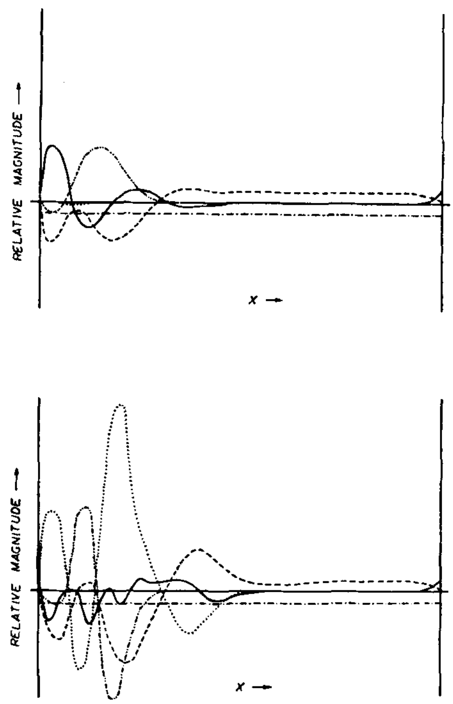

Fig. 16. An east–west cross-section showing the balance of terms in the vorticity equation (6) at a latitude slightly northward of the separation region of the western boundary current, $Y = 0.625$. W_F equals 0.025. *Upper*: $W_I = 0.005$. *Lower*: $W_I = 0.025$. ——, frictional term; – – – –, planetary vorticity tendency; . . . ., advective terms; –.–.–.–, wind stress curl; –..–..–, topographic vorticity tendency.

ary and the outer edge of the shelf. Very near the western boundary the flow is up the slope, but over the major part of the topographic region the flow is toward deeper water. Friction plays an important but complicated role in this entire region, at least for these values of the parameters, W_I and W_F. When $W_I = 0.025$ the structure is quite different. As the meander shown in Figure 10 is crossed, there is an alternation of northward-southward transport as indicated by the planetary vorticity tendency. Similarly the flow is first toward shallower water, then deeper, then shallower. The dynamics of the meandering in terms of conservation of potential vorticity is clearly indicated by the balance between advection of relative vorticity, the planetary vorticity tendency, and the topographic contribution. Over the steep part of the slope, the inertial term is balanced primarily by the topographic term; the meander is a topographic one. As the slope levels out into the deep basin, the inertial term is balanced primarily by the planetary term; the meander is a Rossby wave. The meandering of a particular streamline is a combination of these two. Friction for the most part plays only a minor role in this region.

We summarize these results by describing the motion of a fluid column through one circuit of the ocean. For the *Sverdrup regime* in the southeast part of the ocean, the fluid column moves southward and westward, its planetary vorticity tendency balanced by vorticity input by the wind. As the fluid approaches the boundary, a western boundary current *formation region* is encountered. In the highly frictional case, the fluid column first turns southward in the countercurrent, then turns northward near the boundary. The frictional diffusion of vorticity is balanced by the planetary vorticity tendency. In the highly inertial case, there is no countercurrent, the particle turning directly northward. The planetary vorticity tendency is balanced by vorticity advection. If the particle lies on a streamline which approaches quite close to the boundary, then frictional diffusion becomes important; it is negligible for those streamlines which pass only through the outer edge of the boundary layer. The fluid particle moves northward until it feels the shoaling bottom; the *separation region* is entered. This is a transition region in which the swift, narrow current switches allegiance from the western boundary to the topographic contours and follows them off to the northeast. Friction is important here in both extreme cases, but plays a different role depending upon the size of the inertial parameter, W_I. The situation is quite complex and no simple interpretation is possible. As the fluid particle moves off to the northeast, it enters a *topographic regime* in which horizontal divergence and convergence are of major importance. In the frictional limit the fluid particle follows closely a constant F/H line, entering deeper water as it moves northeastward. Its potential vorticity is nearly conserved, although the relative vorticity is small compared with the Coriolis parameter. Friction and wind stress are negligible. In the highly inertial case, meandering becomes important, and the simple meander theory of Warren has some success. Friction, however, is not negligible everywhere in this region, and even where it is of secondary importance to the advective, topographic, and planetary vorticity terms, it has significant numerical effect such that the fluid particle returns to its starting point in the Sverdrup interior with the proper rotation to match that of the earth. It has accumulated no net vorticity or energy in its travels.

A second series of topographic cases has been studied with the intent of understanding how the steepness of the topographic slope affects the solutions. The topographic regime is that shown in Figure 1. Four solutions have been calculated in which the depth of the western shelf, H_0, has different values while the parameters, W_I and W_F, are held constant. In particular, Figure 17 shows the mass transport streamlines for cases in which H_0 takes on values 0.95, 0.85, 0.75 and 0.50. W_I and W_F are equal to 0.005 and 0.025 respectively.

The first case, for which the bottom slope in the topographic region is equal to $\gamma = (1 - H_0)/\Delta L = 0.4$ (multiplied by D/L to convert back to oceanic dimensions), looks much like the constant depth case, with only slight distortion in the region of variable topography. A western boundary current exists on the shelf, fed by water that flows across the slope region toward the southwest. As the topography becomes steeper (second and third cases in Figure 17, $\gamma = 1.2$ and 2.0 respectively), the streamlines are deflected more and more toward the south in the topographic region until much of the transport reaches the vicinity of the southern boundary, where a highly frictional region is traversed. There the flow turns westward up the slope, but for a very steep slope (fourth case, $\gamma = 4.0$) the water cannot cross the topographic region, instead turning northward to follow topographic contours. No western boundary current forms and the shelf region is one of small motion.

These solutions are rather well predicted by the Topographic–Sverdrup method described earlier, the solutions breaking down only in the vicinity of boundaries (although minor frictional regions occur elsewhere). For small topographic effect ($\gamma = 0.4$) the streamlines pass through an important frictional region near the western boundary, while for large topographic effect ($\gamma = 4.0$), the important frictional region is near the southern boundary. These are the locations at which Topographic–Sverdrup interior streamlines intersect the boundary.

Solutions have been found for cases with larger W_I values, but the streamline patterns vary only in minor detail from those shown, at least for values of $W_I \leqslant 0.025$. The transports in the topographic regions apparently are not large enough for inertial effects to play a very significant role.

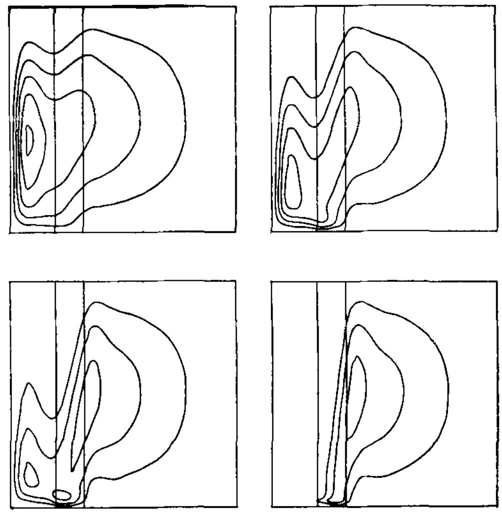

Fig. 17. Mass transport streamlines for four solutions with topographic regimes consisting of a flat shelf of depth H_0 near the western boundary, a slope region of width ΔL and depth gradient $\gamma = (1-H_0)/\Delta L$, and a deep region of unit depth (see Fig. 1). ΔL is equal to 0.125; W_I and W_F are constant and equal to 0.005 and 0.025 respectively. *Upper left*: $H_0 = 0.95$. *Upper right*: $H_0 = 0.85$. *Lower left*: $H_0 = 0.75$. *Lower right*: $H_0 = 0.50$.

Other numerical examples have been studied and the solutions could be discussed in detail, but it is more profitable to just briefly mention some individual cases which bring out points of particular interest. First, let us consider a topographic regime which is not conducive to the formation of meanders. As was pointed out by Rossby (1941) the meander mechanism breaks down for a case in which F/H decreases to the left of the mean stream direction, since in that case the net force on a particle is not a restoring one but of opposite sign. In terms of potential vorticity conservation, the streamline develops curvature (vorticity) of sign opposite to that required to return it to the constant F/H line further downstream, and the path curves away from the F/H lines. As an example, a case was studied for which the topographic contours look like those in Figure 9, but the depth in the northwest corner is *greater* than that to the southeast. For a highly frictional case the western boundary current turns away from the coast when it encounters the down-sloping topography to follow constant F/H lines northeastward into deeper water. Thus a topographic current, in which F/H decreases to the left of the stream, will form. However, when one attempts to solve this problem with larger values of the inertial parameter, it is found that solutions cannot be achieved. The computation becomes unstable and steady solutions cannot be found by our method. It is possible that this behavior means that this topographic situation "encourages" instabilities in the flow, that is, that the flow becomes unstable at smaller Reynolds numbers. It would be of interest to pursue this further, perhaps by solving the time-dependent, initial value problem.

A second study of interest is that of topographic and inertial effects in multiple gyre systems. It was found that it is not possible to isolate gyres in the non-linear, topographic problem as it was in the frictional, constant depth case and that, for a realistic treatment of the wind-driven circulation, entire ocean basins need to be considered. Solutions illustrating why this is true are shown in Figure 18. The wind in all cases is a sinusoidal one with two wind gyres of equal strength present. The upper left solution is the frictional one for a constant depth ocean. The upper right solution is a frictional one in which a topographic slope region is centered about the line $Y = (X + \frac{1}{2})/2$, with deep water to the south and shallow water to the

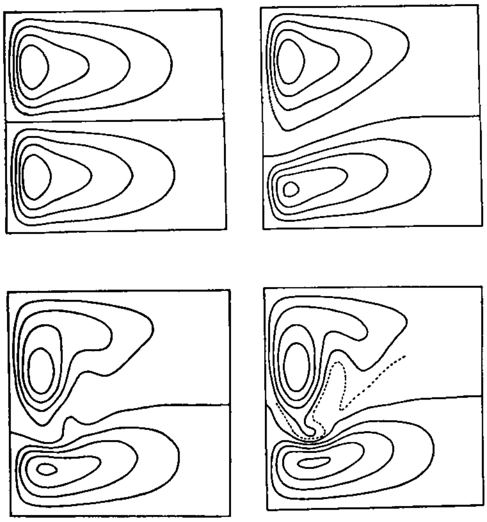

Fig. 18. Mass transport streamlines in an ocean driven by multiple wind systems. The wind stress is given by $\tau = (-\tau_0 \cos 2\pi Y, 0)$. *Upper left*: The solution in an ocean of constant depth. $W_I = 0$ and $W_F = 0.035$. *Upper right*: The solution in an ocean of variable depth in which a narrow shelf extends from $X = 0$, $Y = 0.25$ to $X = 1$, $Y = 0.75$. $W_I = 0$ and $W_F = 0.035$. *Lower left*: Same topography as upper right. $W_I = 0.035$ and $W_F = 0.035$. *Lower right*: Same topography as upper right. $W_I = 0.035$ and $W_F = 0.028$.

north. Thus the western boundary current in the southern gyre leaves shore and water from the northern gyre penetrates southward. The final two cases show solutions to the above problem with increasing non-linearity, such that meanders become quite important, and water from both gyres contribute to the meandering stream. Thus unless the northern and southern boundaries of a given gyre (as determined by the wind pattern) are capable of withstanding normal stresses, that is, there are truly rigid boundaries there, the solutions are not as simple as those discussed earlier in this study. The simplified situation is a useful tool in understanding the nature of topographic and inertial effects but is not adequate in trying to reproduce realistic oceanic transport patterns.

7. Conclusion

In this study we have attempted to understand how topographic effects influence large scale, steady motions in a homogeneous model of the wind-driven ocean circulation. It is clear, however, that there is a rather complicated interaction of the density field and topographic variations in the real ocean, and such a model is useful primarily as a preliminary study to a more realistic system.

The principal results of this investigation have been described in previous sections, but we should summarize here some of the more important observations.

(1) The Topographic–Sverdrup interior is a natural extension of the Sverdrup interior, and this simple dynamical situation is found to govern an extensive part of the model solutions.

(2) The simple, linearized model of the western boundary current discussed in section 4 is found to give qualitatively correct behavior when compared with the numerical solutions. The transition from the frictional Munk solution to the inertial solution of Charney for the formation region of the Gulf Stream is well predicted.

(3) In order to investigate the occurrence of meanders controlled by topography, the transition from a frictional ocean to one in which conservation of potential vorticity plays an important role has been examined. The highly inertial numerical solutions appear to be approaching behavior predicted by the Rossby-topographic meander theory, but it would be interesting to investigate narrower boundary currents so that the scale of the topographic variation is much larger than the width of the meandering stream.

(4) Associated with the meandering stream is a recirculation of water about centers of high pressure, suggesting the possibility that the Gulf Stream, after separation, may exhibit increases and decreases in transport in the downstream direction. In the model these transport variations are of the order of 100%. In addition, it would seem that a meander theory such as Warren's, based upon a stream isolated from its environment, will not be adequate in a more complete description of the free, topographically controlled jet.

(5) Separation of the western boundary current from the coast is an exceedingly complex situation, even for the simple topographic regimes studied, but topographic factors appear to play a dominant role in both the frictional and inertial extremes. It seems possible therefore that this mechanism is indeed involved in the separation phenomenon.

Let us conclude by making a few remarks concerning the techniques and purposes of this investigation. Although, as we have seen, simple analytic models have had some success in describing limited regions of the model ocean, it is apparent that the complexity of the situation requires the use of numerical methods to fit them together properly. This is perhaps the primary usefulness of numerical techniques. Although the solutions by themselves tell us nothing about basic physical processes, we can calculate, for a restricted set of known processes, exceedingly complicated solutions and perhaps decide whether these processes are of importance in a more realistic situation. We seek in this way a qualitative explanation of the gross observational features of the sea.

A major limitation is placed upon the applicability of our simple model to the real ocean by the neglect of baroclinic and time dependent processes and by a lack of knowledge of turbulent diffusion processes. With regard to the former, little can be said at present except that other investigations are in progress which will help to shed light on these phenomena. With regard to the use of a pseudolaminar model to approximate momentum transfer by turbulent processes, we can only argue that these processes may not dominate the dynamical situation and the details of the frictional mechanism may not play an important role. Our solutions show a tendency, at least, in that direction.

Finally, it should be pointed out that the scope of the problem has been restricted not solely to arrive at a problem amenable to analysis but also to achieve a simplicity of interpretation. In a situation already quite complicated it is a distinct advantage to avoid treating systems so complex that some important effects are obscured by others. From the viewpoint of understanding the dynamics of the ocean it would seem better to build gradually upon the hierarchy of existing models by incorporating a single physical process previously neglected.

8. Acknowledgements

This work was supported in part by the Office of Naval Research. I am grateful to Professor Robert S. Arthur, Scripps Institution of Oceanography, for guidance and critical review of this work.

REFERENCES

Bryan, K., 1963. A numerical investigation of a nonlinear model of a wind-driven ocean. *J. Atm. Sci. 20*, 594–606.

Carrier, G. F. & A. R. Robinson, 1962. On the theory of the wind-driven ocean circulation. *J. Fluid Mech. 12*, 49–80.

Charney, J., 1955. The Gulf Stream as an inertial boundary layer. *Proc. Nat. Acad. Sci. Wash. 41*, 731–740.

Conkwright, N. B., 1941. *Introduction to the Theory of Equations*. New York, Ginn and Co., 214.

Fofonoff, N. P., 1954. Steady flow in a frictionless homogeneous ocean. *J. Marin Res. 13*, 254–262.

Fultz, D., 1945. Upper-air Trajectories and Weather Forecasting. *Misc. Report No. 19*, Dept. of Meteorology, University of Chicago, University of Chicago Press.

Greenspan, H., 1962. A criterion for the existence of inertial boundary layers in oceanic circulation. *Proc. Nat. Acad. Sci. 48*, 2034–2039.

Greenspan, H., 1963. A note concerning topography and inertial currents. *J. Marine Res. 21*, 147–154.

Holland, W. R., 1966. Wind-driven circulation in an ocean with bottom topography. Ph.D. dissertation, Scripps Institution of Oceanography, 123 pp.

Il'in, A. M. & V. M. Kamenkovich, 1963. On the influence of friction on the ocean circulation. *Doklady Akad. Nauk., SSSR 150*, 1274–1277.

Moore, D. W., 1963. Rossby waves in ocean circulation. *Deep Sea Res. 10*, 735–747.

Morgan, G. W., 1956. On the wind-driven ocean circulation. *Tellus 8*, 301–320.

Munk, W. H., 1950. On the wind-driven ocean circulation. *J. Met. 7*, 79–93.

Rossby, C. G., 1940. Planetary flow patterns in the atmosphere. *Roy. Met. Soc., Quart. Jour. 66* (suppl), 68–87.

Stommel, H., 1948. The westward intensification of wind-driven ocean currents. *Trans. Am. Geoph. Union 29*, 202–206.

Sverdrup, H. U., 1947. Wind-driven currents in a baroclinic ocean; with application to the equatorial currents of the eastern Pacific. *Proc. Nat. Acad. Sci. Wash. 33*, 318–326.

Thom, A. & C. J. Apelt, 1961. *Field Computations in Engineering and Physics*. New York, Van Nostrand, 165 pp.

Veronis, G., 1966. Wind-driven ocean circulation—Part 2. Numerical solutions of the non-linear problem. *Deep Sea Res. 13*, 31–56.

Warren, B. A., 1963. Topographic influences on the path of the Gulf Stream. *Tellus 15*, 167–183.

Welander, P., 1959. On the vertically integrated mass transport in the oceans. *The Atmosphere and Sea in Motion*. Bert Bolin, Editor. New York, Rockefeller Institute Press, pp. 95–101.

О ВОЗБУЖДАЕМОЙ ВЕТРОМ ЦИРКУЛЯЦИИ В ОКЕАНЕ С УЧЕТОМ ТОПОГРАФИИ ДНА

Исследуется влияние топографии дня на возбуждаемую ветром океаническую циркуляцию для однородной модели на β-плоскости со стационарным вихрем напряжений ветра. Линейная модель, изучавшаяся Манком (1950), и нелинейная модель изучавшаяся Кэриером и Робинсоном (1962) являются частными случаями, так же как и простая модель, предложенная Уорреном (1963) для описания меандров Гольфстрима. Хотя эффекты стратификации плотности не учитываются, включены инерционный эффект и эффект трения и определяются решения для различных типов топографии.

Изучены простые аналитические модели и найдено, что они полезны в описании ограниченных областей океанического бассейна. В частности, концепция внутреннего режима, когда нелинейные члены и члены с трением несущественны, может быть распространена на случай переменной глубины. В областях с сильным инерционным потоком над дном с учетом топографии, простая модель меандра, исследованная Россби (1940), имеет некоторую успешность в предсказании пути потока. В обеих моделях важность изоплет постоянного F/H, где F — параметр Кориолиса и H — глубина, демонстрируется путем показа сильной тенденции линий тока следовать этим изоплетам или меандрировать около этих кривых.

Находятся полные численные решения для конечноразностного уравнения вихря с помощью эффективной реалксационной схемы, предложенной для этой цели. Результаты показывают, что реакция океана может строго контролироваться формой океанического дна и что такие крупные особенности океанической циркуляции, как отделение Гольфстрима, меандрирование и переменный перенос, могут быть связаны с эффектами топографии дна.